Low-grade chronic inflammation in regions of the normal mouse arterial intima predisposed to atherosclerosis

Jenny Jongstra-Bilen,[1,2] Mehran Haidari,[1,3] Su-Ning Zhu,[1,3] Mian Chen,[1,3] Daipayan Guha,[1] and Myron I. Cybulsky[1,3]

[1]Toronto General Research Institute, University Health Network, Toronto, Ontario M5G 2C4, Canada
[2]Department of Immunology and [3]Department of Laboratory Medicine and Pathobiology, University of Toronto, Toronto, Ontario M5S 1A8, Canada

Atherosclerotic lesions develop in regions of arterial curvature and branch points, which are exposed to disturbed blood flow and have unique gene expression patterns. The cellular and molecular basis for atherosclerosis susceptibility in these regions is not completely understood. In the intima of atherosclerosis-predisposed regions of the wild-type C57BL/6 mouse aorta, we quantified increased expression of several proinflammatory genes that have been implicated in atherogenesis, including vascular cell adhesion molecule–1 (VCAM-1) and a relative abundance of dendritic cells, but only occasional T cells. In contrast, very few intimal leukocytes were detected in regions resistant to atherosclerosis; however, abundant macrophages, including T cells, were found throughout the adventitia (Adv). Considerably lower numbers of intimal CD68$^+$ leukocytes were found in inbred atherosclerosis-resistant C3H and BALB/c mouse strains relative to C57BL/6 and 129; however, leukocyte distribution throughout the Adv of all strains was similar. The predominant mechanism for the accumulation of intimal CD68$^+$ cells was continued recruitment of bone marrow–derived blood monocytes, suggestive of low-grade chronic inflammation. Local proliferation of intimal leukocytes was low. Intimal CD68$^+$ leukocytes were reduced in VCAM-1–deficient mice, suggesting that mechanisms of leukocyte accumulation in the intima of normal aorta are analogous to those in atherosclerosis.

CORRESPONDENCE
Myron Cybulsky:
myron.cybulsky@utoronto.ca

Abbreviations used: Adv, adventitia; ANOVA, analysis of variance; DT, descending thoracic aorta; GC and LC, greater curvature and lesser curvature, respectively, of the ascending aortic arch; HRP, horseradish peroxidase; IAO, intercostal artery ostia; ICAM-2, intercellular adhesion molecule–2; LDL, low density lipoprotein; LOX-1, lectin-like oxidized LDL receptor–1; MCP-1, monocyte chemotactic protein–1; PI, propidium iodide; RAM, rabbit antimacrophage; VCAM-1, vascular cell adhesion molecule–1.

With the recent rise in obesity and related conditions in North America, atherosclerosis is likely to remain a major cause of morbidity and mortality for the coming decades. Understanding the underlying mechanisms for the onset of this disease may provide new strategies for delaying or preventing thrombotic complications associated with advanced atherosclerosis.

Atherosclerosis is initiated and accelerated by systemic risk factors such as elevated low density lipoprotein (LDL), hypertension, high blood sugar, and oxidation products from smoking. Although the entire vascular endothelium is exposed to these stimuli, atherosclerotic lesions develop preferentially at bifurcations, branch points, and inner curvatures of arteries, suggesting that local factors contribute to disease susceptibility. It is widely accepted that the complex patterns of blood flow in these regions expose the endothelium to "disturbed" hemodynamic forces (shear stress), and these may induce the expression of proinflammatory genes (1–3). Our previous experiments in normocholesterolemic C57BL/6 mice focused on the transcription factor NF-κB and showed priming as well as a low level of activation of this signal transduction pathway in endothelial cells located in atherosclerosis-susceptible regions of the ascending aorta (4). Consistent with these findings, the expression level of vascular cell adhesion molecule–1 (VCAM-1) was elevated in atherosclerosis-predisposed regions of the rabbit or mouse aorta, but was lower relative to expression induced by various inflammatory stimuli (4–6). Recent gene profiling experiments with endothelial cells of the normal porcine aorta showed relative up-regulation of several other proinflammatory genes in the aortic arch, such as those of

J. Jongstra-Bilen and M. Haidari contributed equally to this work.

M. Haidari's present address is Atherosclerosis Research Lab, Texas Heart Institute, Houston, TX 77030.

The online version of this article contains supplemental material.

cytokines IL-1, IL-6, or the chemokine monocyte chemotactic protein–1 (MCP-1), as well as antioxidative genes, including glutathione peroxidase or microsomal glutathione S-transferase 2 (7). In addition, changes in cell shape and proliferation or lipoprotein transport and retention in the intima were reported in atherosclerosis-susceptible regions (4, 8–12), underscoring the dramatic biological changes that accompany the low-grade expression of proinflammatory genes in these areas. Consistent with the up-regulation of chemokines and adhesion molecules in the lesion-prone areas, intimal leukocytes were found preferentially at several branch points of the normal rabbit aorta and in human carotid bifurcations, where accumulation of macrophages, dendritic cells, and T cells was reported (8, 13, 14). However, the abundance of these leukocytes in atherosclerosis-predisposed versus -resistant regions and their relationship with atherosclerosis susceptibility have not been determined.

Genetic factors contribute to atherogenesis. In humans, it is well known that family history predicts cardiovascular events. Susceptibility to atherosclerosis also differs amongst inbred strains of mice. For instance, when fed an atherogenic diet, the susceptible C57BL/6 mice develop lesions in the aortic root (15), and apolipoprotein E–deficient mice in the C57BL/6 background develop larger areas of lesions than in the resistant BALB/c or C3H/HeJ backgrounds (16, 17). Understanding the molecular basis for genetic susceptibility will likely lead to the identification of key elements that contribute to the development of atherosclerosis. Previous studies showed a correlation between endothelial cell responses to systemic risk factors and the genetic susceptibility of mice to atherosclerotic lesion formation (18, 19).

Mouse models have led to an understanding of key molecules involved in atherosclerotic lesion formation. They have demonstrated a critical role for proinflammatory genes, including various adhesion molecules and chemokines such as VCAM-1 and MCP-1, which mediate the accumulation of leukocytes in arterial lesions (20, 21). Our hypothesis is that arterial biology at lesion-predisposed regions of the normal intima recapitulates aspects of the inflammatory response in atherosclerosis, although at a lesser magnitude. The same molecules may mediate leukocyte recruitment and accumulation in the normal intima, and this inflammatory milieu may contribute to atherosclerotic lesion formation on introduction of atherosclerotic risk factors.

In this study, we demonstrated that in the normal intima, regions predisposed to atherosclerosis expressed relatively higher levels of several proinflammatory genes that have been implicated in atherogenesis and contained an abundance of dendritic cells. In contrast, macrophages and T cells were abundant throughout the entire adventitia (Adv). These data demonstrate for the first time that cellular composition and distribution are different in the intima and the Adv. The correlation between susceptibility to atherosclerosis and abundance of intimal (not adventitial) myeloid cells was not only topographic but also extended to strains with different genetic susceptibilities to atherosclerosis. We also demonstrated that bone marrow–derived monocytes are recruited to the normal aortic intima and showed that the accumulation of intimal $CD68^+$ cells is dependent on the expression of VCAM-1. These data demonstrate low-grade chronic inflammation in atherosclerosis-predisposed regions of the normal arterial intima and suggest that mechanisms contributing to this process are analogous to those found in atherosclerosis.

RESULTS

Proinflammatory genes are expressed in the normal intima of an atherosclerosis-prone region of the ascending aortic arch

We previously used immunostaining to demonstrate increased expression of VCAM-1 in endothelial cells located in regions of the mouse and rabbit aorta that are predisposed to atherosclerotic lesion formation (4, 5). In this study, a real-time PCR approach was adopted to broaden the scope of gene expression by intimal cells in these regions, improve sensitivity, and obtain more quantitative data. Aortae of WT C57BL/6 mice were perfused, pinned opened, and, after a brief collagenase treatment intimal cells (cells above the internal elastic lamina), were isolated using a dissecting microscope. Levels of mRNA in the lesser curvature and greater curvature of the ascending aortic arch (LC and GC, respectively), regions with high and low probability for atherosclerosis, respectively (4, 5), were directly examined. We found that mRNA

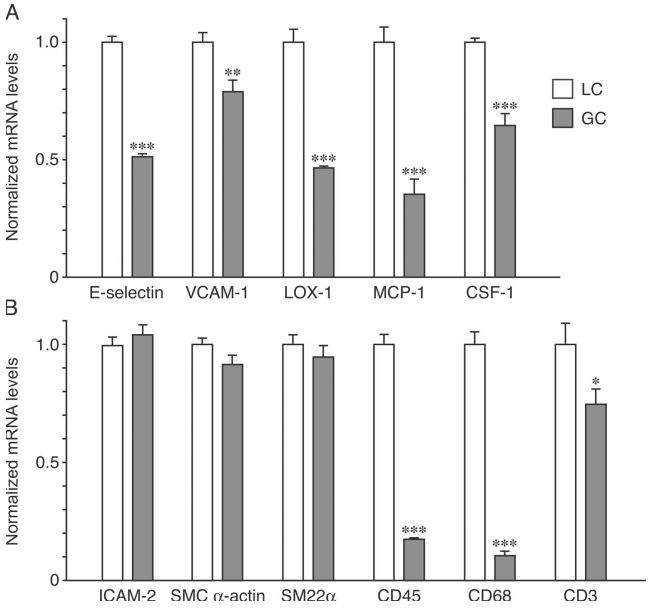

Figure 1. Comparison of intimal cell gene expression in regions of the normal C57BL/6 mouse ascending aorta with different susceptibility to atherosclerosis. Real-time PCR was used to determine the mRNA levels of proinflammatory (A) and cell marker (B) genes. Expression levels for each gene were normalized to CD31, and GC values were compared with the respective LC values (see Supplemental materials and methods). The mean ± SEM of eight independent experiments is plotted. ***, $P < 0.001$; **, $P < 0.01$; and *, $P < 0.05$, indicating significant differences between LC and GC values for each gene using the unpaired *t* test.

levels of adhesion and proinflammatory molecules E-selectin, VCAM-1, lectin-like oxidized LDL receptor–1 (LOX-1), MCP-1, and CSF-1 were expressed at significantly higher levels in the LC relative to the GC (Fig. 1 A). One interpretation of these data is that this pattern of mRNA expression represents differential gene expression by endothelial cells. This is likely the case for E-selectin, an adhesion molecule that is expressed selectively by endothelial cells. However, VCAM-1 can be expressed by endothelial and smooth muscle cells (22), LOX-1 can be expressed by these cells as well as macrophages (23, 24), and chemokines/growth factors can be expressed by a variety of cells, including leukocytes. Therefore, differences in the abundance of intimal smooth muscle cells and leukocytes may also be responsible.

We therefore investigated the abundance of intimal smooth muscle cells and leukocytes in the LC and GC of the mouse ascending aortic arch. Real-time PCR experiments did not reveal differences in mRNA levels for the endothelial intercellular adhesion molecule–2 (ICAM-2) or for the smooth muscle cell markers SMCα-actin and SM22α; however, mRNA levels of the panleukocyte marker CD45 were elevated more than fivefold in the LC (Fig. 1 B). These data suggest that in contrast to vascular smooth muscle cells, increased numbers of leukocytes are present in the intima of the LC. Levels of CD68, a myeloid cell marker, were elevated by >9-fold in the LC intima, whereas T cell marker CD3 levels were increased by only 1.5-fold (Fig. 1 B). These data suggest that cells of the myeloid lineage are more abundant in the LC intima relative to GC. Because these cells can produce numerous cytokines and growth factors, they may contribute to the elevated mRNA levels of LOX-1, MCP-1, and CSF-1 that were found in the LC of the ascending arch.

Intimal myeloid cells, but not T cells, are abundant in atherosclerosis-susceptible regions of the aorta

En face immunoconfocal microscopy experiments were performed to determine the nature and abundance of

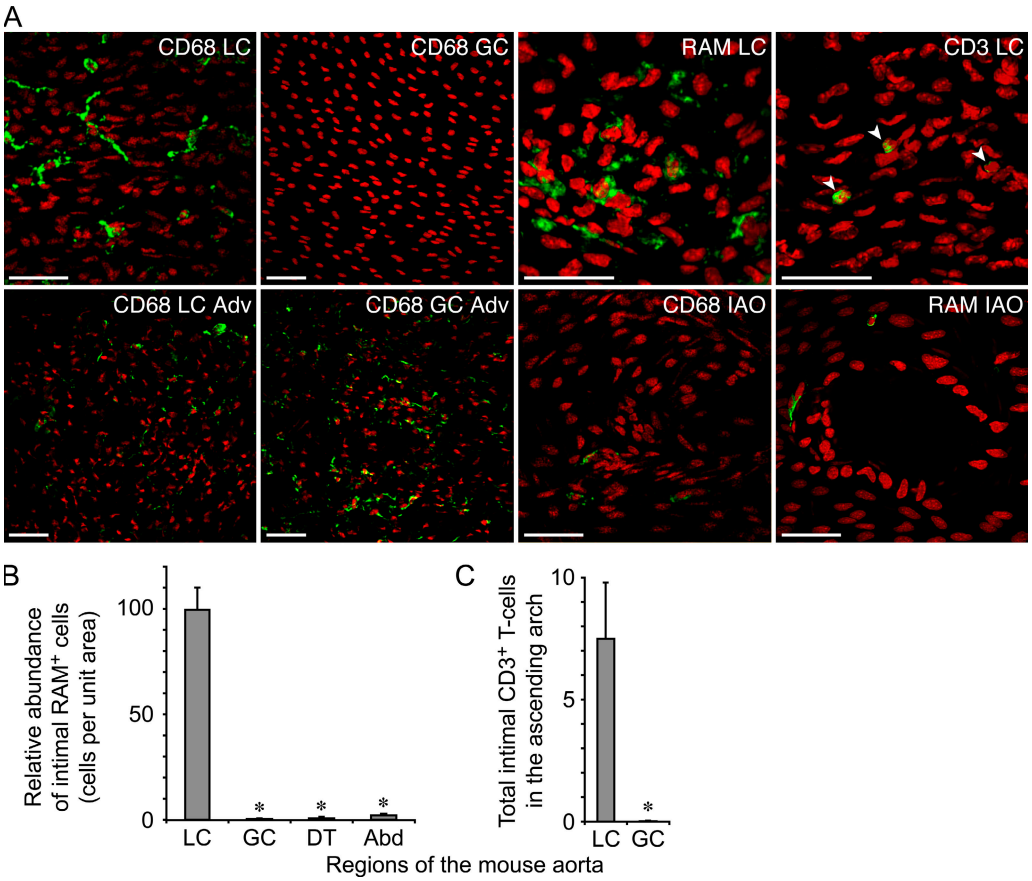

Figure 2. The distribution and abundance of leukocytes in regions of the normal mouse aorta with different susceptibilities to atherosclerosis. (A) Shown are representative immunoconfocal images of the intima in the LC and GC of the ascending aorta, the Adv in these regions, and the IAO in the DT. Segments of aorta were stained with antibodies directed to CD68, macrophages (RAM) or CD3 (green), and nuclei were counterstained with PI (red). At a minimum, four experiments were performed with each antibody. Bars, 50 μm. (B) The relative densities of RAM^+ cells in the LC, GC, DT, and abdominal (Abd) aorta are shown. Means ± SEM of four experiments were normalized to LC values, which are represented as 100. (C) Total number of $CD3^+$ T cells found in the LC and GC of the ascending aorta. Means ± SEM of four experiments are plotted. *, $P < 0.001$, indicating significant differences from the LC value using the unpaired *t* test.

leukocytes in the aorta. Regions susceptible or resistant to developing lesions were examined, and the intima was compared with the corresponding Adv. Representative data are shown in Fig. 2 A. The intima in the lesion-resistant GC was readily distinguishable from the lesion-susceptible LC by the shape, orientation, and density of propidium iodide (PI)–stained nuclei. GC nuclei were evenly spaced, oval shaped, and oriented at the direction of blood flow, whereas nuclei in the LC appeared irregular and randomly oriented. These differences are consistent with endothelial cell shape changes in response to disturbed blood flow (25), which were readily detectable in the silver nitrate–stained samples depicted in Fig. S1 (available at http://www.jem.org/cgi/content/full/jem.20060245/DC1). The density of intimal cell nuclei in the LC appeared higher than in the GC (Fig. 2 A). To determine if this was caused by differences in endothelial cell numbers or leukocytes accumulated in the LC, we quantified the endothelial cells and nuclei in the LC, GC, and descending thoracic aorta (DT). This analysis revealed that the number of endothelial cells (identified by

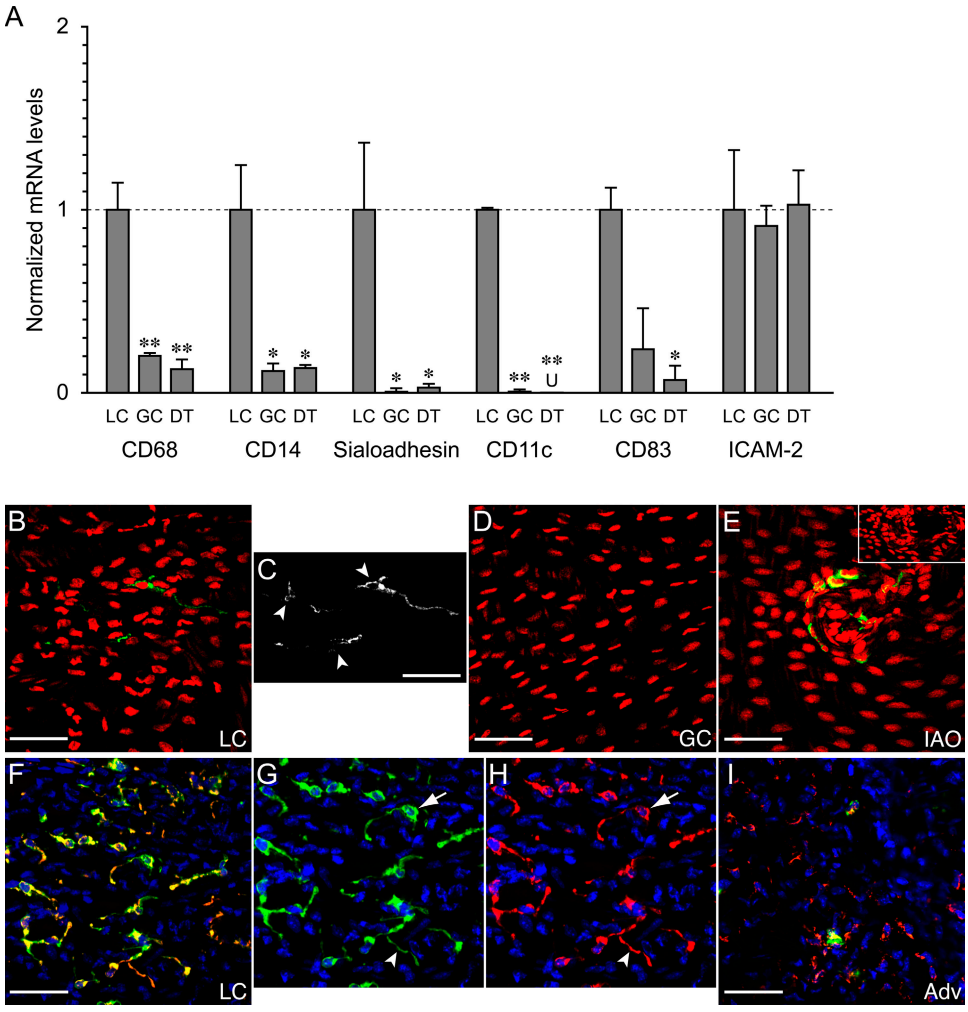

Figure 3. Expression of macrophage and dendritic cell marker genes in the aortic intima. (A) Relative gene expression levels determined by real-time PCR were derived from three or four independent experiments, as described in Fig. 1 for the LC, GC, and DT. The dashed line represents the normalized LC value of 1. Means ± SEM are shown. *, $P < 0.05$; and **, $P < 0.01$, indicating significant differences from LC values using one-way ANOVA (except for CD11c, which used the unpaired *t* test). U, undetectable mRNA levels. Note that similar values were obtained when a different normalizer gene than CD31, HPRT (reference 44) was used (Fig. S3). (B–E) Representative en face immunoconfocal microscopy images from three independent experiments show CD11c expression (green) and nuclei (red) in intimal cells. The same LC region is shown in B and C, with only the fluorescein channel shown in C. Arrowheads indicate cell bodies. The GC and IAO are shown in D and E, respectively. (E, inset) Staining with nonimmune hamster IgG (negative control) is shown. (F) A representative immunoconfocal microscopy image from two independent experiments shows intimal cells in the LC region coexpressing CD68 (red, Cy3) and CD11c (green, fluorescein). The fluorescein (G) and Cy3 (H) channels corresponding to the image in F are shown independently, and cell bodies and processes that show more intense staining for CD11c (arrows) and CD68 (arrowheads) are indicated. (I) A representative image of the Adv shows predominance of CD68 staining and costaining for CD68 and CD11c in only occasional cells. Bars, 50 μm.

Table I. Number of nuclei or endothelial cells (EC) and nuclear density in different segments of mouse aorta

	Nuclei/mm^2	EC/mm^2	Density[a]
LC	3,415 ±74.4[b, c] n[d] = 6	2,431 ± 57.8 n = 12	1.40
GC	2,691 ± 88.91 n = 3	2,685 ± 93.25 n = 10	1.00
DT	2,657 ± 103.3 n = 3	2,549 ± 148.4 n = 4	1.04

[a]Nuclei/EC.
[b]Mean ± SE.
[c]$P < 0.001$ when compared with the EC number in LC.
[d]Total number of areas counted.

staining of cell junctions with silver nitrate) was comparable in all regions (Table I and Fig. S1). In the GC and DT, the number of nuclei (identified by staining with PI) was identical to endothelial cells, whereas in the LC it was 1.4-fold higher (Table I). These data demonstrate that intimal leukocytes account for increased nuclear density observed in the LC.

Numerous CD68$^+$ and rabbit antimacrophage (RAM)–positive cells were found in the LC intima, whereas the GC region was essentially devoid of these cells (Fig. 2 A). CD68$^+$ and RAM$^+$ intimal cells were also observed in other atherosclerosis-susceptible regions, such as intercostal artery ostia (IAO; Fig. 2 A), celiac, mesenteric, and renal artery ostia, and in the aortic root (not depicted). CD68$^+$ or RAM$^+$ cells were present very rarely in straight segments of the DT and abdominal aorta. These observations were supported by quantifying the relative abundance of intimal RAM$^+$ cells in different regions of the aorta (Fig. 2 B). Real-time PCR studies detected more abundant mRNA expression of macrophage markers, CD14, and sialoadhesin, in addition to CD68, in intimal cells of the LC relative to the GC and straight segments of the DT, excluding IAO (Fig. 3 A and Fig. S3, available at http://www.jem.org/cgi/content/full/jem.20060245/DC1). The combined immunoconfocal and real-time PCR data demonstrated that resident intimal myeloid cells, including monocytes/macrophages, accumulate preferentially in regions of the aorta that are susceptible to atherosclerosis in WT normocholesterolemic mice.

In contrast to differences in the arterial intima, the Adv of both the LC and GC regions harbored abundant CD68$^+$ (Fig. 2 A) or RAM$^+$ (not depicted) cells. These data indicate that the accumulation of myeloid cells in lesion-prone areas applies only to the intimal layer. Intimal CD3$^+$ T cells were occasionally found in the LC of the arch (Fig. 2 A). On average, only seven or eight cells were observed in the entire LC intima of the ascending aorta (Fig. 2 C), in contrast to several hundred CD68$^+$ cells found in the same region (see Figs. 5 and 7). T cells were abundant in the Adv throughout the aorta (not depicted), which was consistent with a recent report (26).

Dendritic cells constitute the majority of myeloid cells accumulated in atherosclerosis-susceptible regions of the intima

CD68 is expressed by monocytes/macrophages, dendritic cells, and several other cell types (27–30). Because we observed that CD68$^+$ intimal cells frequently extended long, dendritic-like processes (Fig. 2 A), we investigated if intimal myeloid cells also express dendritic cell markers. Real-time PCR studies revealed that mRNA levels of CD11c, a pan-dendritic cell marker, were elevated by >100-fold in the LC region relative to the GC and straight segments of the DT, where levels were barely detectable or undetectable (Fig. 3 A and Fig. S3). CD83, a marker for mature dendritic cells (31, 32), also appeared elevated in the LC region, but a statistically significant difference was observed only between the LC and the DT (Fig. 3 A). ICAM-2 expression was similar in all regions. Elevated expression in the LC region of CD11c was confirmed by immunoconfocal microscopy. Abundant intimal CD11c$^+$ cells with extended dendrites were found in the LC and near ostia of intercostal arteries of the DT but not the GC (Fig. 3, B–E). To assess the proportion of CD68$^+$ cells that were also CD11c$^+$, segments of the aorta were stained with antibodies against both antigens simultaneously. The majority of intimal CD68$^+$ cells costained positive for CD11c (Fig. 3, F–H). Some cells stained more intensely for CD68 (red, as indicated by arrowheads), whereas in others CD11c staining (green, indicated by arrows) was brighter. Costaining for CD11c of most CD68$^+$ cells was also prevalent in the intima adjacent to IAO (Fig. S2 A, available at http://www.jem.org/cgi/content/full/jem.20060245/DC1). Intimal CD68$^+$ cells were rarely weakly positive or negative for CD11c. On the other hand, only occasional CD68$^+$ cells in the Adv stained brightly for CD11c cells (Fig. 3 I), and these cells lacked the long dendritic processes. The specificity of staining with each antibody was verified in control experiments (Fig. S2). Based on costaining of CD68$^+$ cells for CD11c and the presence of long dendrites, we concluded

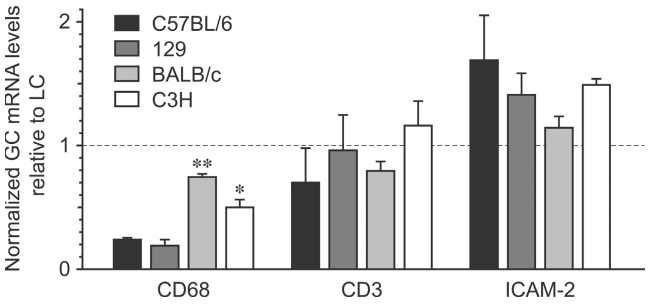

Figure 4. Expression of CD68, CD3, and ICAM-2 by intimal cells isolated from the GC and LC regions of the ascending aorta from different strains of mice. Real-time PCR was used as described in Fig. 1. The GC/LC ratios obtained in different strains were compared. The dashed line represents the normalized LC value of 1. Means ± SEM are plotted for three or four experiments (C57BL/6, 129, and C3H strains) or eight experiments (BALB/c strains). *, $P < 0.01$; and **, $P < 0.001$, indicating significant differences from the C57BL/6 strain using one-way ANOVA.

that the majority of CD68$^+$ cells in the intima are dendritic cells, whereas in the Adv these cells are rare.

The abundance of intimal CD68$^+$ cells correlates with strain susceptibility to atherosclerosis

Having found that the abundance of CD68$^+$ cells in the intima of the normal mouse aorta correlates with the spatial susceptibility to lesion formation, we investigated whether a correlation also exists with strain susceptibility to atherosclerosis. We compared the highly susceptible C57BL/6 strain to BALB/c and C3H, which are relatively resistant, and 129, which has intermediate susceptibility (16). Using real-time PCR, we determined the ratio of CD68 mRNA expression in atherosclerosis resistant to susceptible regions of the ascending aorta. In C57BL/6 and 129 strains, the CD68 expression ratio was significantly lower than in the atherosclerosis-resistant BALB/c and C3H strains (Fig. 4). In contrast, differences were not found in the expression ratios of CD3 and ICAM-2. PCR data were supported by en face immunoconfocal analyses, which showed lower numbers of intimal CD68$^+$ cells in the LC of C3H versus C57BL/6 mice (Fig. 5 A) and very infrequent CD68$^+$ cells in the GC of all strains. Similarly, lower numbers of intimal CD68$^+$ cells were observed in the LC of BALB/c versus C57BL/6 mice (unpublished data). In the LC of C57BL/6 mice, intimal CD68$^+$ cells extended from the aortic root to the arch (areas A, B, and C in Fig. 5, B and C), whereas in C3H mice these cells were found most consistently in the midportion of the LC (area B in Fig. 5, B and C). In some instances, intimal CD68$^+$ cells were rarely seen in areas A and C of C3H mice. Despite these differences, CD68$^+$ cells

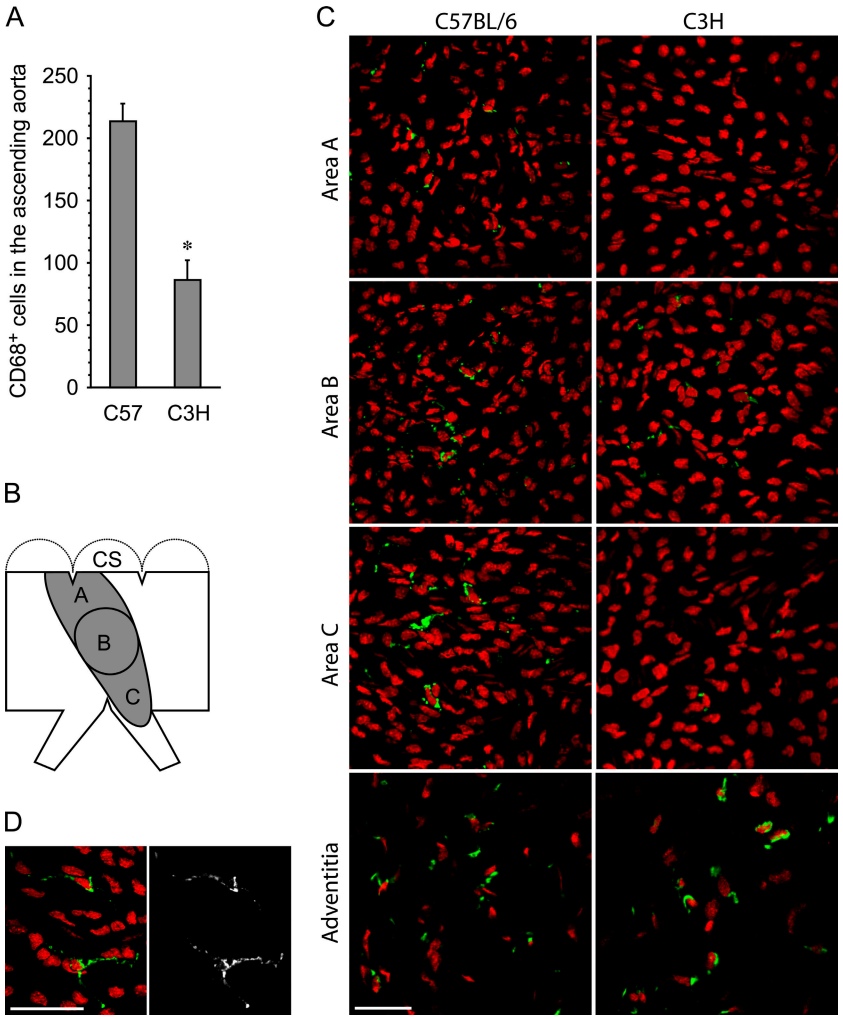

Figure 5. Immunoconfocal assessment of the abundance and distribution of intimal CD68$^+$ cells in the ascending aorta of normal C57BL/6 and C3H mice. (A) The number of intimal CD68$^+$ cells in the LC of C57BL/6 (C57) and C3H mice is plotted. Means ± SEM for four experiments are shown. *, $P < 0.001$ using the unpaired *t* test. CD68$^+$ cells were detected very infrequently in the GC of both strains. (B) A schematic diagram of the en face ascending aorta indicating areas A, B, and C of the LC (shaded area). The coronary sinus (CS) and three valve leaflets are indicated. (C) Representative images of C57BL/6 and C3H mice aortae examine the abundance of CD68$^+$ cells (green) and nuclei (red) in areas A–C of the LC intima and Adv. (D) Prominent CD68$^+$ dendritic-like processes are evident in a high magnification view of a C3H LC intima (left, green; right, fluorescein channel only). Bars, 50 μm.

in the intima of C3H mice exhibited similar morphological features, including long dendritic-like processes (Fig. 5 D), and nuclei in the LC region were irregularly oriented. The abundance of $CD68^+$ cells in the Adv was indistinguishable between the two strains (Fig. 5 C), further supporting the notion that the correlation between abundance of $CD68^+$ cells and predisposition to atherosclerosis is restricted to the intimal layer.

Intimal dendritic cells are derived predominantly from the bone marrow

The accumulation of intimal dendritic cells in regions of the aorta predisposed to atherosclerosis may result from local proliferation, recruitment of bone marrow–derived monocytes from the blood, or both. To address these possibilities, BrdU labeling experiments were performed in C57BL/6 mice. BrdU has a short half-life, and cells undergoing DNA synthesis (S phase of the cell cycle) are labeled only within the first hour after BrdU injection (33, 34). The bone marrow is a site of monocytopoiesis, which is enhanced by hypercholesterolemia in swine (35), and mouse bone marrow myeloid $Gr\text{-}1^-$ progenitors and immature neutrophils that express low levels of Gr-1 can be labeled with BrdU (36). Using flow cytometry, we found that 13% of the total bone marrow–nucleated cells were labeled with BrdU 2 h after i.p. injection, and 25% of $Mac\text{-}1^+Gr\text{-}1^-$ and 22% of $Mac\text{-}1^+Gr\text{-}1^{int}$ myeloid precursors were labeled. These data are consistent with a published report (36). Fig. 6 A shows a typical time course of labeled leukocyte appearance in the blood after a single BrdU injection. Labeled leukocytes were not detected in the blood at 2 h. Therefore, we assessed local cell proliferation in the aorta at this time point and detected only occasional $BrdU^+$ nuclei in the LC region (Fig. 6 B). BrdU-labeled monocytes ($Mac\text{-}1^+Gr\text{-}1^{int}$) were detected in the blood between 8 and 24 h, whereas labeled neutrophils ($Mac\text{-}1^+Gr\text{-}1^{high}$) and T cells ($CD3^+$) did not circulate during this time frame (Fig. 6 A). A significant increase in $BrdU^+$ nuclei was observed in the LC region 24 h after BrdU injection (Fig. 6, B and C), indicating that $BrdU^+$ monocytes were recruited to the LC intima. $BrdU^+$ nuclei were not detected in the GC, whereas occasional labeled cells (approximately six or seven) were found in the entire Adv of the arch at 24 h but not at 2 h. Based on these data, we concluded that low-grade recruitment of blood monocytes is the predominant mechanism for dendritic cell accumulation in the normal intima of regions predisposed to atherosclerosis.

Accumulation of $CD68^+$ cells in the intima of the LC is dependent on VCAM-1 expression

The adhesion molecule VCAM-1 participates in the formation of early atherosclerotic lesions in hypercholesterolemic mice (37, 38), and we demonstrated that its expression is elevated in the LC of the ascending aorta of normal mice (see Fig. 1 and [4]). We undertook to determine if the accumulation of intimal $CD68^+$ cells in atherosclerosis-predisposed regions of the normal aorta is dependent on VCAM-1. Using en face immunoconfocal microscopy, we compared the number of intimal $CD68^+$ cells in the LC of VCAM-1–deficient mice ($Vcam\text{-}1^{D4D/D4D}$) with corresponding WT littermates. These mice were bred over 10 generations into the C57BL/6 background. Intimal $CD68^+$ cells were significantly lower in $Vcam\text{-}1^{D4D/D4D}$ mice (Fig. 7, A–C). Interestingly, the observed differences between $Vcam\text{-}1^{D4D/D4D}$ and WT mice were found only in the intima and not the Adv (Fig. 7, D and E), indicating that VCAM-1 participates in the

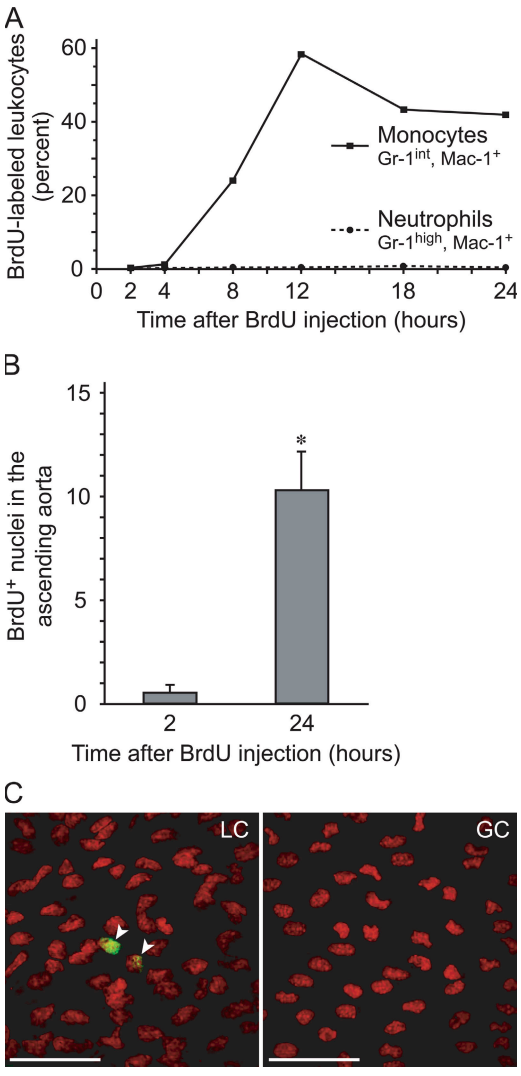

Figure 6. Analysis of $BrdU^+$ leukocytes in blood and the ascending aorta of C57BL/6 mice. (A) Blood leukocytes stained with anti-BrdU, anti-CD11b, and anti–Gr-1 were analyzed by flow cytometry for the presence of $BrdU^+$ monocytes and neutrophils at different times after injection of BrdU. (B) The number of $BrdU^+$ nuclei in the intimal layer of the LC at 2 and 24 h after BrdU injection was determined by immunoconfocal microscopy. Each bar represents the mean ± SEM of four experiments. *, $P < 0.05$, using the unpaired *t* test. (C) Representative en face immunoconfocal images of the intima 24 h after BrdU injection demonstrate $BrdU^+$ nuclei (arrowheads) in the LC (left) but not the GC (right). Bars, 50 μm.

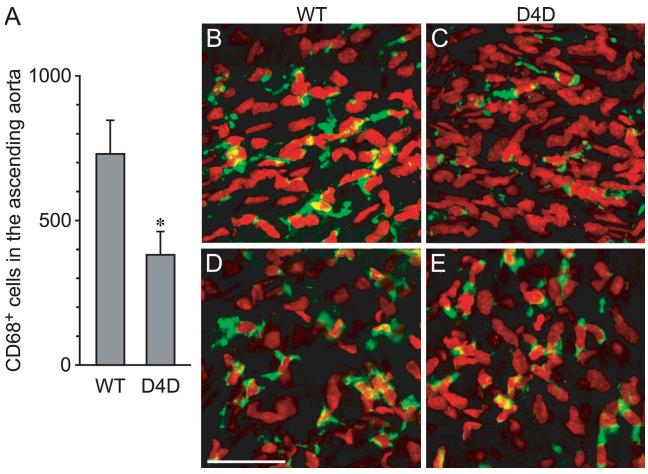

Figure 7. Immunoconfocal assessment of the abundance and distribution of intimal CD68$^+$ cells in the ascending aorta of WT and *Vcam1*$^{D4D/D4D}$ (D4D) mice. (A) The numbers of intimal CD68$^+$ cells in the LC are plotted. Means ± SEM for four pairs of WT and D4D littermates are shown. *, $P < 0.01$, using the paired two-tailed *t* test. (B–E) Representative en face immunoconfocal images of the intima (B and C) and corresponding Adv (D and E) in the LC in WT (B and D) and D4D (C and E) mice. All images are at the same magnification. Bar, 50 μm.

accumulation of CD68$^+$ cells in the arterial intima but not in the Adv.

DISCUSSION

In this study, real-time PCR and en face immunoconfocal microscopy revealed spatial and quantitative correlations between dendritic cells residing in distinct regions of the normal aortic intima and the expression of proinflammatory genes, the topography of atherosclerotic lesion formation, and the genetic susceptibility of mice to atherogenesis. In contrast to the intima, leukocytes were abundant throughout the entire Adv in all mouse strains and were not found in the media. Our observations are in agreement with a study that revealed intimal macrophages near ostia of the rabbit aorta (8); however, we demonstrated that most intimal myeloid cells have dendrites and express dendritic cell markers. We also showed that the composition of myeloid cells in the intima is different from the Adv because relatively few adventitial myeloid cells express CD11c.

In humans, macrophages, dendritic cells, and CD3$^+$ T cells were found in the atherosclerosis-prone arterial intima of healthy children (14, 39, 40). Wick et al. called these sites vascular-associated lymphoid tissue based on the notion that the abundance of antigen-presenting cells and T cells implicates their involvement in local immune surveillance against potentially harmful antigens (13). A protective role for intimal dendritic cells has not been established in humans or mice. We observed relatively few intimal CD3$^+$ T cells in the mouse aorta, which suggests that if mouse intimal dendritic cells encounter pathogens, they either exit the intima and migrate to organized lymphoid tissues or initiate a local inflammatory response that recruits T cells. We observed abundant myeloid cells and T cells throughout the aortic Adv of normocholesterolemic C57BL/6 mice, which was consistent with a recent study by Galkina et al. (26). The formation of organized lymphoid tissues in the Adv during hypercholesterolemia (26) may be part of the immune response to modified lipoproteins that modulates disease progression. Throughout the normal Adv, lymphocytes are recruited via the microvasculature (26), which suggests that these microvessels are not subjected to local regulation by factors that predispose distinct regions of the intima to atherosclerosis.

We observed considerable differences in the abundance of CD68$^+$ cells located in atherosclerosis-predisposed regions of the aortic intima in atherosclerosis-susceptible versus-resistant strains of mice, yet adventitial myeloid cells were abundant in all strains. This suggests that the abundance of intimal myeloid cells is most likely caused by strain-specific gene expression by luminal endothelial cells rather than differences in global responses to inflammatory stimuli or intrinsic macrophage and dendritic cell defects. In support of this, Shi et al. demonstrated that chemotactic activity in conditioned media and MCP-1 protein secretion in response to modified forms of LDL were substantially lower in cultures of aortic endothelial cells isolated from atherosclerosis-resistant C3H relative to susceptible C57BL/6 mice (19). Thus, it is conceivable that the endothelium in atherosclerosis-predisposed regions of the aorta from resistant strains have attenuated responses to the local hemodynamic environment, resulting in lower levels of proinflammatory stimuli and reduced accumulation of intimal macrophages.

There is evidence that during atherogenesis both the recruitment of monocytes from the blood and cell proliferation in the intima contribute to the accumulation of macrophages in atherosclerotic lesions (41, 42). Our BrdU experiments in normocholesterolemic mice demonstrated that the proliferation rate of the resident intimal cells was very low. This is in agreement with previous experiments with normal rabbits (8). We also demonstrated that bone marrow–derived monocytes are recruited from the blood into the normal intima in regions predisposed to atherosclerosis. The expression of proinflammatory genes, such as VCAM-1, E-selectin, and MCP-1, may account for this low-grade inflammation. In support of this hypothesis, considerably lower numbers of CD68$^+$ intimal leukocytes were found in normocholesterolemic VCAM-1–deficient mice as compared with WT littermates. In the setting of hypercholesterolemia, VCAM-1 contributes to the formation of early atherosclerotic lesions (37, 38). These suggest that parallel molecular mechanisms underlie chronic inflammation in atherosclerosis-susceptible regions of the normal aorta and in early atherosclerosis; however, inflammation in normal and atherosclerotic vessels differs in magnitude.

Based on the close spatial and strain correlations between intimal dendritic cells and atherogenesis in mice, we propose that when systemic risk factors such as hypercholesterolemia are introduced, intimal dendritic cells promote

atherosclerotic lesion formation and contribute to the unique topographic distribution of lesions. Close correlations between areas of enhanced permeability to serum proteins and intimal mononuclear cell accumulations were described (43), and it is likely that intimal myeloid cells may readily accumulate oxidatively modified lipoproteins, become activated, and secrete proinflammatory factors that initiate and amplify an inflammatory response. In addition to a pathogenic role, the cellular composition of the intima may serve as a predictive marker for atherosclerosis. Future studies will investigate the potential functions of intimal dendritic cells.

MATERIALS AND METHODS

Mice. Female and male C57BL/6, 129X1/SvJ (129/SvJ, termed 129), and BALB/c strains, as well as the C3.SW-H2b/SnJ congenic strain (designated C3H), were used at ages between 3–6 mo. *Vcam1*$^{D4D/D4D}$ mice and WT littermates (in the C57BL/6 background) were generated by heterozygous intercrosses and used at the age of 12 mo. Mice were bred and housed at the University Health Network Animal Facility and were fed standard rodent chow. All procedures were performed according to the guidelines of the Canadian Council on Animal Care.

Antibodies and reagents. RAM antiserum (Accurate Chemical); biotin-conjugated anti–mouse antibodies targeting CD11c, CD3, GR-1 (BD Biosciences), and CD68 (Serotec); FITC–anti-BrdU, –anti-CD11c (BD Biosciences), and PE–anti-CD11b (Caltag Laboratories) antibodies and secondary antibodies; biotin–anti–rabbit IgG (Jackson ImmunoResearch Laboratories); and antifluorescein–horseradish peroxidase (HRP; Invitrogen) were used. BrdU and PI were purchased from Sigma-Aldrich, TOTO-3 was obtained from Invitrogen, a BrdU detection kit was purchased from BD Biosciences, and Tyramide signal amplification kits (TSA, Fluorescein, or Cyanine3) were obtained from PerkinElmer. All the reagents for real-time PCR, including the TaqMan gene expression assay mix for LOX-1, MCP-1, CSF-1, CD14, CD11c, CD83, and sialoadhesin were purchased from Applied Biosystems.

En face immunoconfocal microscopy of the aorta. Mice were perfused at 100 mm Hg via the left ventricle with ice-cold PBS for 5 min followed by 4% paraformaldehyde in PBS for 10 min. Aortae were harvested, and the surrounding adipose tissue was dissected while immersed in cold PBS. After further fixation in 4% paraformaldehyde for 30 min at 4°C, and permeabilization with 0.2% Triton X-100 and 0.1 M glycine in PBS for 7 min at 22°C, single or double immunostaining was performed according to the guidelines of the Tyramide amplification kit. Essentially, after quenching endogenous peroxidase activity with 3% H_2O_2, tissue segments were incubated with anti-CD32/-CD16 Fc-block (1:100; BD Biosciences) and 10 μg/ml nonimmune mouse IgG (Sigma-Aldrich) and IgG corresponding to the species of the primary antibody. Primary antibodies (for single or double staining) were incubated overnight at 4°C. Negative controls included isotype control IgG of the appropriate species. Incubation with biotinylated secondary antibodies for 1 h at 22°C was performed if the primary antibody was not biotin conjugated. Samples were then incubated with streptavidin-HRP, followed by FITC-conjugated Tyramide. For double staining for CD68 and CD11c, Cy3-Tyramide was used in conjunction with biotin–anti-CD68. After quenching the remaining HRP activity with 1% H_2O_2, 1 μg/ml anti-FITC–HRP (for 30 min) and FITC-Tyramide were used to reveal FITC–anti-CD11c staining. Nuclei were stained with 2 μg/ml PI or 0.2 μM TOTO-3 for single or double staining, respectively. The arch was opened in a highly reproducible manner (5), and other segments were cut longitudinally. Flattened segments of the aorta were mounted on glass slides with mounting media (Dako Fluorescent; DakoCytomation). En face immunofluorescence images were obtained with confocal microscopes, one (MRC-1024ES; Bio-Rad Laboratories) equipped with a krypton/argon laser and 40× or 60× (NA 1.4) oil objectives (Nikon), and the other (Flowview FV-1000; Olympus) equipped with 40× (NA 1.0) and 60× (NA 1.4) oil objectives (Olympus).

Silver nitrate staining of endothelial cell junctions. Mouse aortas were pressure perfused via the left ventricle with PBS for 5 min, followed by $AgN0_3$ (0.125% in H_2O) for 30 s, PBS for 1 min, and 4% paraformaldehyde for 10 min.

Real-time PCR and primers synthesis. Gene expression was assessed using real-time PCR only in intimal cells isolated from the LC, GC, and DT regions of the mouse thoracic aorta (see Supplemental materials and methods, available at http://www.jem.org/cgi/contente/full/jem.20060245/DC1). Primers (TaqMan MGB probes; Applied Biosystems) were purchased or designed (see Table S1, available at www.jem.org/cgi/content/full/jem.20060245/DC1) using software (Primer Express; Applied Biosystems). The SM22α and SMCα-actin primers were provided by S. Hanada and M. Husain (Toronto General Research Institute, Toronto, Canada). Real-time PCR reactions were performed using the default PCR cycle on a sequence detection system (ABI Prism 7900 HT; Applied Biosystems), and amplified DNA was detected by SYBR Green (Applied Biosystems) incorporation or measurement of fluorogenic signal from FAM-labeled TaqMan MGB probes. Dissociation curve analyses were performed to confirm specificity of the SYBR Green signals in each experiment. Quantification of relative amounts of genes of interest was performed using software (Sequence Detection Systems 2.0; Applied Biosystems) and the comparative standard curve method or the C_t method when the efficiency of primers was comparable. Data were normalized to CD31 or the housekeeping gene HPRT, and gene expression in the GC and DT regions were compared with the LC (see Supplemental materials and methods).

BrdU injections and analysis of blood leukocytes by flow cytometry. Mice were injected i.p. with 2 mg BrdU (0.2 ml diluted in sterile PBS). Approximately 0.1 ml of blood was collected from the retro-orbital plexus, and bone marrow cells were collected from femurs. Leukocytes were surface stained for Mac-1, Gr-1, and CD3 after lysis of red blood cells. Staining of nuclei with anti-BrdU antibodies was performed after fixing/permeabilizing the cells and digesting with DNase I according to the protocol provided in the BrdU flow kit (BD Biosciences). Analyses were performed with a flow cytometer (EPICS-XL; Beckman Coulter).

Statistical analyses. The unpaired and paired *t* tests were used when comparing differences between two groups. In experiments with multiple groups, differences were first evaluated using one-way analysis of variance (ANOVA), and the Tukey-Kramer multiple comparison test was used to determine differences between pairs.

Online supplemental material. Supplemental materials and methods provides. Fig. S1 depicts an analysis of endothelial cells and nuclei in the LC and GC regions of the ascending arch. Fig. S2 shows double staining of the intimal cells of IAO with CD68 and CD11c and the corresponding controls. Fig. S3 depicts the expression of macrophage and dendritic cell marker genes in the aortic intima. Table S1 provides the sequence of primers designed for real-time PCR. Online supplemental material is available at http://www.jem.org/cgi/content/full/jem.20060245/DC1.

We thank the Banting and Best Diabetes Centre and the Toronto General Research Institute for contributing to the purchase of the ABI Prism 7900 HT real-time PCR machine.

This research was supported primarily by Heart and Stroke Foundation of Ontario (HSFO) grant T-5125 (to M.I. Cybulsky). Support was also provided by HSFO grant T-5480 (to M.I. Cybulsky), and grant RGPIN 194609-3 from the Natural Sciences and Engineering Research Council of Canada to J. Jongstra-Bilen. M.I. Cybulsky is a Career Investigator of the HSFO and a member of the Heart and Stroke/Richard Lewar Centre of Excellence at the University of Toronto, which provided fellowship support for M. Haidari.

The authors have no conflicting financial interests.

Submitted: 31 January 2006
Accepted: 12 July 2006

REFERENCES

1. Brooks, A.R., P.I. Lelkes, and G.M. Rubanyi. 2002. Gene expression profiling of human aortic endothelial cells exposed to disturbed flow and steady laminar flow. *Physiol. Genomics*. 9:27–41.
2. Gimbrone, M.A., Jr., T. Nagel, and J.N. Topper. 1997. Biomechanical activation: an emerging paradigm in endothelial adhesion biology. *J. Clin. Invest*. 100:S61–S65.
3. Garcia-Cardena, G., J. Comander, K.R. Anderson, B.R. Blackman, and M.A. Gimbrone Jr. 2001. Biomechanical activation of vascular endothelium as a determinant of its functional phenotype. *Proc. Natl. Acad. Sci. USA*. 98:4478–4485.
4. Hajra, L., A.I. Evans, M. Chen, S.J. Hyduk, T. Collins, and M.I. Cybulsky. 2000. The NF-kappa B signal transduction pathway in aortic endothelial cells is primed for activation in regions predisposed to atherosclerotic lesion formation. *Proc. Natl. Acad. Sci. USA*. 97:9052–9057.
5. Iiyama, K., L. Hajra, M. Iiyama, H. Li, M. DiChiara, B.D. Medoff, and M.I. Cybulsky. 1999. Patterns of vascular cell adhesion molecule-1 and intercellular adhesion molecule-1 expression in rabbit and mouse atherosclerotic lesions and at sites predisposed to lesion formation. *Circ. Res*. 85:199–207.
6. Nakashima, Y., E.W. Raines, A.S. Plump, J.L. Breslow, and R. Ross. 1998. Upregulation of VCAM-1 and ICAM-1 at atherosclerosis-prone sites on the endothelium in the ApoE-deficient mouse. *Arterioscler. Thromb. Vasc. Biol*. 18:842–851.
7. Passerini, A.G., D.C. Polacek, C. Shi, N.M. Francesco, E. Manduchi, G.R. Grant, W.F. Pritchard, S. Powell, G.Y. Chang, C.J. Stoeckert Jr., and P.F. Davies. 2004. Coexisting proinflammatory and antioxidative endothelial transcription profiles in a disturbed flow region of the adult porcine aorta. *Proc. Natl. Acad. Sci. USA*. 101:2482–2487.
8. Malinauskas, R.A., R.A. Herrmann, and G.A. Truskey. 1995. The distribution of intimal white blood cells in the normal rabbit aorta. *Atherosclerosis*. 115:147–163.
9. Schwenke, D.C., and T.E. Carew. 1989. Initiation of atherosclerotic lesions in cholesterol-fed rabbits. I. Focal increases in arterial LDL concentration precede development of fatty streak lesions. *Arteriosclerosis*. 9:895–907.
10. Schwenke, D.C., and T.E. Carew. 1989. Initiation of atherosclerotic lesions in cholesterol-fed rabbits. II. Selective retention of LDL vs. selective increases in LDL permeability in susceptible sites of arteries. *Arteriosclerosis*. 9:908–918.
11. Schwenke, D.C. 1995. Selective increase in cholesterol at atherosclerosis-susceptible aortic sites after short-term cholesterol feeding. *Arterioscler. Thromb. Vasc. Biol*. 15:1928–1937.
12. Napoli, C., F.P. D'Armiento, F.P. Mancini, A. Postiglione, J.L. Witztum, G. Palumbo, and W. Palinski. 1997. Fatty streak formation occurs in human fetal aortas and is greatly enhanced by maternal hypercholesterolemia. Intimal accumulation of low density lipoprotein and its oxidation precede monocyte recruitment into early atherosclerotic lesions. *J. Clin. Invest*. 100:2680–2690.
13. Wick, G., M. Romen, A. Amberger, B. Metzler, M. Mayr, G. Falkensammer, and Q. Xu. 1997. Atherosclerosis, autoimmunity, and vascular-associated lymphoid tissue. *FASEB J*. 11:1199–1207.
14. Millonig, G., H. Niederegger, W. Rabl, B.W. Hochleitner, D. Hoefer, N. Romani, and G. Wick. 2001. Network of vascular-associated dendritic cells in intima of healthy young individuals. *Arterioscler. Thromb. Vasc. Biol*. 21:503–508.
15. Nishina, P.M., S. Lowe, J. Verstuyft, J.K. Naggert, F.A. Kuypers, and B. Paigen. 1993. Effects of dietary fats from animal and plant sources on diet-induced fatty streak lesions in C57BL/6J mice. *J. Lipid Res*. 34:1413–1422.
16. Smith, J.D., D. James, H.M. Dansky, K.M. Wittkowski, K.J. Moore, and J.L. Breslow. 2003. In silico quantitative trait locus map for atherosclerosis susceptibility in apolipoprotein E-deficient mice. *Arterioscler. Thromb. Vasc. Biol*. 23:117–122.
17. Tian, J., H. Pei, J.C. James, Y. Li, A.H. Matsumoto, G.A. Helm, and W. Shi. 2005. Circulating adhesion molecules in apoE-deficient mouse strains with different atherosclerosis susceptibility. *Biochem. Biophys. Res. Commun*. 329:1102–1107.
18. Shi, W., N.J. Wang, D.M. Shih, V.Z. Sun, X. Wang, and A.J. Lusis. 2000. Determinants of atherosclerosis susceptibility in the C3H and C57BL/6 mouse model: evidence for involvement of endothelial cells but not blood cells or cholesterol metabolism. *Circ. Res*. 86:1078–1084.
19. Shi, W., M.E. Haberland, M.L. Jien, D.M. Shih, and A.J. Lusis. 2000. Endothelial responses to oxidized lipoproteins determine genetic susceptibility to atherosclerosis in mice. *Circulation*. 102:75–81.
20. Cybulsky, M.I., D. Won, and M. Haidari. 2004. Leukocyte recruitment to atherosclerotic lesions. *Can. J. Cardiol*. 20(Suppl. B):24B–28B.
21. Hansson, G.K. 2005. Inflammation, atherosclerosis, and coronary artery disease. *N. Engl. J. Med*. 352:1685–1695.
22. Li, H., M.I. Cybulsky, M.A. Gimbrone Jr., and P. Libby. 1993. Inducible expression of vascular cell adhesion molecule-1 by vascular smooth muscle cells in vitro and within rabbit atheroma. *Am. J. Pathol*. 143:1551–1559.
23. Kume, N., and T. Kita. 2001. Lectin-like oxidized low-density lipoprotein receptor-1 (LOX-1) in atherogenesis. *Trends Cardiovasc. Med*. 11:22–25.
24. Yoshida, H., N. Kondratenko, S. Green, D. Steinberg, and O. Quehenberger. 1998. Identification of the lectin-like receptor for oxidized low-density lipoprotein in human macrophages and its potential role as a scavenger receptor. *Biochem. J*. 334:9–13.
25. Gerrity, R.G., M. Richardson, J.B. Somer, F.P. Bell, and C.J. Schwartz. 1977. Endothelial cell morphology in areas of in vivo Evans blue uptake in the aorta of young pigs. II. Ultrastructure of the intima in areas of differing permeability to proteins. *Am. J. Pathol*. 89:313–334.
26. Galkina, E., A. Kadl, J. Sanders, D. Varughese, I.J. Sarembock, and K. Ley. 2006. Lymphocyte recruitment into the aortic wall before and during development of atherosclerosis is partially L-selectin dependent. *J. Exp. Med*. 203:1273–1282.
27. Strobl, H., C. Scheinecker, E. Riedl, B. Csmarits, C. Bello-Fernandez, W.F. Pickl, O. Majdic, and W. Knapp. 1998. Identification of CD68+lin− peripheral blood cells with dendritic precursor characteristics. *J. Immunol*. 161:740–748.
28. Andreeva, E.R., I.M. Pugach, and A.N. Orekhov. 1997. Subendothelial smooth muscle cells of human aorta express macrophage antigen in situ and in vitro. *Atherosclerosis*. 135:19–27.
29. Pulford, K.A., A. Sipos, J.L. Cordell, W.P. Stross, and D.Y. Mason. 1990. Distribution of the CD68 macrophage/myeloid associated antigen. *Int. Immunol*. 2:973–980.
30. Randolph, G.J., S. Beaulieu, S. Lebecque, R.M. Steinman, and W.A. Muller. 1998. Differentiation of monocytes into dendritic cells in a model of transendothelial trafficking. *Science*. 282:480–483.
31. Berchtold, S., P. Muhl-Zurbes, C. Heufler, P. Winklehner, G. Schuler, and A. Steinkasserer. 1999. Cloning, recombinant expression and biochemical characterization of the murine CD83 molecule which is specifically upregulated during dendritic cell maturation. *FEBS Lett*. 461:211–216.
32. Wolenski, M., S.O. Cramer, S. Ehrlich, C. Steeg, G. Grossschupff, K. Tenner-Racz, P. Racz, B. Fleischer, and A. von Bonin. 2003. Expression of CD83 in the murine immune system. *Med. Microbiol. Immunol. (Berl.)*. 192:189–192.
33. Goto, Y., J.C. Hogg, T. Suwa, K.B. Quinlan, and S.F. van Eeden. 2003. A novel method to quantify the turnover and release of monocytes from the bone marrow using the thymidine analog 5′-bromo-2′-deoxyuridine. *Am. J. Physiol. Cell Physiol*. 285:C253–C259.
34. Kriss, J.P., and L. Revesz. 1962. The distribution and fate of bromodeoxyuridine and bromodeoxycytidine in the mouse and rat. *Cancer Res*. 22:254–265.
35. Averill, L.E., R.C. Meagher, and R.G. Gerrity. 1989. Enhanced monocyte progenitor cell proliferation in bone marrow of hyperlipemic swine. *Am. J. Pathol*. 135:369–377.
36. Basu, S., G. Hodgson, M. Katz, and A.R. Dunn. 2002. Evaluation of role of G-CSF in the production, survival, and release of neutrophils from bone marrow into circulation. *Blood*. 100:854–861.
37. Cybulsky, M.I., K. Iiyama, H. Li, S. Zhu, M. Chen, M. Iiyama, V. Davis, J.C. Gutierrez-Ramos, P.W. Connelly, and D.S. Milstone. 2001. A major role for VCAM-1, but not ICAM-1, in early atherosclerosis. *J. Clin. Invest*. 107:1255–1262.

38. Dansky, H.M., C.B. Barlow, C. Lominska, J.L. Sikes, C. Kao, J. Weinsaft, M.I. Cybulsky, and J.D. Smith. 2001. Adhesion of monocytes to arterial endothelium and initiation of atherosclerosis are critically dependent on vascular cell adhesion molecule-1 gene dosage. *Arterioscler. Thromb. Vasc. Biol.* 21:1662–1667.
39. Millonig, G., G.T. Malcom, and G. Wick. 2002. Early inflammatory-immunological lesions in juvenile atherosclerosis from the Pathobiological Determinants of Atherosclerosis in Youth (PDAY)-study. *Atherosclerosis.* 160:441–448.
40. Bobryshev, Y.V., and R.S. Lord. 1995. Ultrastructural recognition of cells with dendritic cell morphology in human aortic intima. Contacting interactions of vascular dendritic cells in athero-resistant and atheroprone areas of the normal aorta. *Arch. Histol. Cytol.* 58:307–322.
41. Lessner, S.M., H.L. Prado, E.K. Waller, and Z.S. Galis. 2002. Atherosclerotic lesions grow through recruitment and proliferation of circulating monocytes in a murine model. *Am. J. Pathol.* 160:2145–2155.
42. Orekhov, A.N., E.R. Andreeva, I.A. Mikhailova, and D. Gordon. 1998. Cell proliferation in normal and atherosclerotic human aorta: proliferative splash in lipid-rich lesions. *Atherosclerosis.* 139:41–48.
43. Gerrity, R.G., H.K. Naito, M. Richardson, and C.J. Schwartz. 1979. Dietary induced atherogenesis in swine. Morphology of the intima in prelesion stages. *Am. J. Pathol.* 95:775–792.
44. de Kok, J.B., R.W. Roelofs, B.A. Giesendorf, J.L. Pennings, E.T. Waas, T. Feuth, D.W. Swinkels, and P.N. Span. 2005. Normalization of gene expression measurements in tumor tissues: comparison of 13 endogenous control genes. *Lab. Invest.* 85:154–159.